Dalton Transactions

PAPER

View Article Online
View Journal | View Issue

Cite this: *Dalton Trans.*, 2016, **45**, 9920

Physicochemical aspects of epoxide driven nano-ZrO_2 hydrogel formation: milder kinetics for better properties†

V. Oestreicher,[a] M. Perullini*[a] and M. Jobbágy*[a,b]

Received 22nd January 2016,
Accepted 25th February 2016

DOI: 10.1039/c6dt00323k

www.rsc.org/dalton

Robust and highly transparent quasi amorphous ZrO_2-water-glycerol hydrogels were obtained in a mild one pot procedure, based on the 2,3-epoxy-1-propanol driven alkalinization. SAXS-based characterization of the sol–gel transition revealed that an homogeneously nucleated sol composed of 2 nm primary particles continuously grows up to a critical size of 5–6 nm, when gelation takes place. These particles reach a size of 8–10 nm, depending on the Zr(IV) concentration. Conductivity measurements offer an overall *in situ* assessment of the reaction rate. The gelled samples share a common trend: once the conductivity decays to 40% of the starting value, the primary particles nucleate and when this decay reaches 20%, the sol–gel transition takes place. The mild conditions employed herein prevent massive ripening and recrystallization leaving hydrogels with extremely low undesired visible light scattering. This suitable nanostructure was achieved in a wide range of total Zr(IV) concentrations or water to glycerol ratios.

1. Introduction

For decades, inorganic hydrogels revealed great potential in materials science as precursors of highly textured monolithic oxides, either in the form of aerogels or xerogels.[1] More recently, pristine hydrogels, typically based on SiO_2, demonstrated to be suitable matrices to develop advanced biomaterials,[2] including enzyme[3] or living cell loaded hybrid phases.[4–7] Moreover, if the mechanical and/or optical properties of these hydrogels are properly tuned,[8] advanced biosensing,[9,10] bioremediating,[11] photosynthetic[12] or biosynthetic devices[13] can be envisaged. Beyond SiO_2 based hydrogels, certain alternative Al(III),[14] Fe(III)[15] or Zr(IV)[16] based-matrices were introduced in the search for enhanced functionalities. Most of these hydrogels were based on the pH-driven coagulation of preformed nanoparticles, in order to prevent harmful synthesis conditions (alcohol, acids, *etc.*). However, both their mechanical and optical properties were poor compared to *in situ* gelled polymeric SiO_2 obtained by the well-established alcohol-free sol–gel process.[8] Then, alternative routes for developing novel hydrogels are highly desirable. More than a decade ago, Gash *et al.*[17,18] developed several transition and main-group metal-based hydrogels based on the homogeneous alkalinization of metallic salt solutions. This alternative route to the alkoxide-based sol–gel process also succeeded in the synthesis of oxo-hydroxide colloids[19] and advanced monoliths.[19–21] Among the obtained phases, we focused our attention on ZrO_2 based hydrogels, as suitable substitutes for SiO_2-based hydrogels. However, first attempts based on the use of propylene oxide reported fast alkalinization/gelation kinetics (in the scale of a few seconds), resulting mostly in opaque, brittle and inhomogeneous phases.[22,23] Moreover, the involved reactions developed autogenous heating.[24] More recently, it was proposed to use milder precursors as $ZrOCl_2$ instead of the highly acidic $ZrCl_4$; this oxolated precursor holds the inherent advantage of requiring only two equivalents of base per mol of Zr(IV) to develop ZrO_2.[25] However, suitable gelation rates (and suitable physical properties) were only achieved with an extra addition of a strong acid, returning to an undesired aggressive condition in the starting reaction batch.

In the present study, a milder route for the preparation of robust ZrO_2-based hydrogels is proposed, employing glycerol–water mixtures as reaction media. The obtained solids are analyzed in terms of the alkalinization/gelation kinetics as well as the structural evolution along the sol–gel transition.

2. Experimental

2.1. Synthesis of hydrogels and conductivity measurements

$ZrOCl_2{\cdot}8H_2O$ was dissolved in glycerol/water solutions; the samples were labeled as ZXGY, where X represents the approximate

[a]*INQUIMAE, DQIAQF, Facultad de Ciencias Exactas y Naturales, Universidad de Buenos Aires, Pabellón II, Ciudad Universitaria, C1428EHA-Buenos Aires, Argentina. E-mail: mercedesp@qi.fcen.uba.ar, jobbag@qi.fcen.uba.ar*
[b]*Centro Interdisciplinario de NanoCiencia y NanoTecnología, Argentina*
†Electronic supplementary information (ESI) available: ESI figures. See DOI: 10.1039/c6dt00323k

Table 1 Sample codes, composition and gelation time, t_{gel}. Asterisk (*) denotes reversible gelation

Sample	$ZrOCl_2$/M	Epoxide/M	t_{gel}/min
Z1.0G2	0.08	0.32	—
Z2.5G2	0.20	0.80	*
Z5.0G2	0.40	1.60	13.05 ± 0.05
Z7.5G2	0.60	2.40	5.91 ± 0.03
Z10G2	0.80	3.20	1.11 ± 0.01
Z5.0G1	0.40	0.80	59.55 ± 0.07
Z5.0G3	0.40	2.40	7.65 ± 0.03

weight in volume percentage of ZrO_2 in the resulting hydrogels and Y represents the ratio of epoxide to Zr(IV) with respect to the stoichiometric amount (see Table 1). These parent solutions were transferred to a container equipped with a conductometric/thermal probe Thermo ORION 162A under vigorous stirring. A calibration curve was recorded (at 298 K) employing solutions of $ZrOCl_2$ salt in a typical solvent mixture, in order to ensure a linear response in the concentration range of the parent solutions. The whole reactor was immersed in a stirred water bath (100 times higher in volume) thermostatized at 298 K. The initial time was triggered once an appropriate amount of 2,3-epoxy-1-propanol (epoxide in the following) was added to the mixture. The gelation time was estimated as the time until the magnetic stirrer stopped after epoxide addition.

2.2. Characterization of solids

The microstructure characterization was performed at the LNLS SAXS2 beamline in Campinas, Brazil, working at λ = 0.1488 nm, with the wave vector range 0.09 $nm^{-1} < q <$ 2.2 nm^{-1}. All the hydrogel samples showed isotropic scattering and were modeled as a bi-continuous non-particular system[26] characterized by a correlation length (ξ) and a characteristic domain size (d), according to the Teubner and Strey phenomenological model. Free software SASfit version 0.94.6 was used to fit experimental data. Intensity profiles show a peak at

$$q_{max} = \sqrt{\left(\frac{2\pi}{d}\right)^2 - \left(\frac{1}{\xi}\right)^2}$$

Representative samples were characterized by powder X-ray diffraction (PXRD) using graphite-filtered Cu K_α radiation (λ = 1.5406 Å). The samples were measured with a step size of 0.2 degrees and a step time of 2 s.

3. Results and discussion

3.1. Epoxide driven alkalinization kinetics

It is known that epoxide driven alkalinization depends on several factors, including solvent composition, as well as the nucleophile and epoxide nature.[27,28] The process is based on the counteranion's (typically chloride) nucleophilic attack onto the epoxide ring and the subsequent formation of halohydrin, driving a net pH rise up to basic conditions (eqn (1)).[29,30] The epoxide method requires an excess of epoxide with respect to

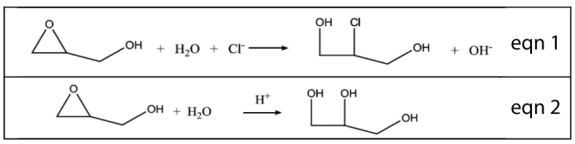

Scheme 1 Epoxide ring's rupture and alkalinization (eqn (1)) and epoxide's hydrolysis in acid media (eqn (2)).

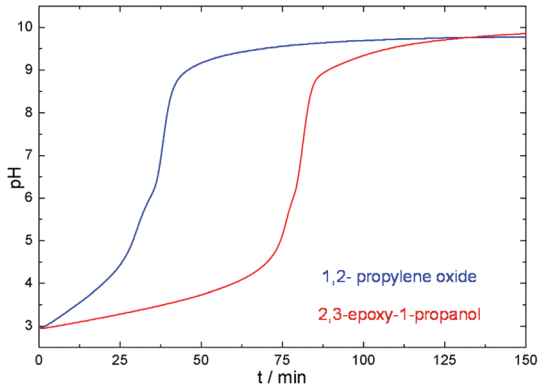

Fig. 1 Evolution of pH at 298 K recorded for aqueous solutions containing 2,3-epoxy-1-propanol (red) or 1,2-propylene oxide (blue) 0.15 M in the presence of NaCl 0.15 M.

the cation concentration. In addition to the alkalinization reaction (eqn(1)), part of the starting epoxide equivalents is consumed by hydrolysis (eqn (2)); this undesired reaction becomes relevant if the process takes place under high water activity (Scheme 1).

In the present study, 2,3-epoxy-1-propanol was chosen as the epoxide and chloride as the nucleophile. The former was reported to be a milder alternative to the commonly employed 1,2-propylene oxide, while its lower vapor pressure ensures proper handling under ambient conditions. Fig. 1 depicts the alkalinization profiles of both epoxides in aqueous media, reaching a basic condition (pH = 9.50). Taking the time to reach neutral pH as the reference, the 2,3-epoxy-1-propanol driven alkalinization rate is three-fold slower than the 1,2-propylene oxide alkalinization rate.

3.2. Gelation

The hydrogels were prepared by adding 2,3-epoxy-1-propanol (epoxide)-glycerol solutions to aqueous solutions containing increasing concentrations of $ZrOCl_2$. The water content in each sample was fixed as 70% of the total volume of the reaction mixture. Sample codes and final compositions are compiled in Table 1.

After a previous screening, it was concluded that a two-fold stoichiometric amount of epoxide (four moles per mole of Zr(IV)) ensures massive ZrO_2 formation. This epoxide to Zr(IV) ratio was employed in most of the cases; higher epoxide to Zr(IV) ratios make the gelation kinetics of concentrated samples extremely fast hindering the structural characterization along the sol–gel transition.

As shown in Fig. 2, conductivity measurements during the reaction revealed that for the samples Z2.5G2 to Z10G2, a massive decay to a 10% of the initial value took place within the time span ranging from minutes to hours. However, sample Z1.0G2 stabilized at a 20% of the initial value; a similar behavior was observed during the gelation of sample Z5.0G1 (see Fig. S1, ESI†), suggesting that the epoxide concentration was limiting in these cases.

For most of the samples, gelation times followed a dependence with the reagent's concentration expectable for the employed reaction (see Fig. 3).[29] The inverse of gelation time is proportional to the alkalinization rate, that is proportional to the product of chloride and epoxide initial concentrations, $[epoxide]_o[Cl^-]_o$.

However, for the highest Zr(IV) content (sample Z10G2) an extremely fast process took place, and hence it was excluded from the aforementioned analysis. Interestingly, that particular sample resulted in a marked initial temperature jump of almost 8 K along the first minute of the reaction (see Fig. S2, ESI†). Temperature jumps are common for these highly enthalpic processes (ring rupture coupled with an acid base reaction). A moderate temperature rise of 10 K results in a markedly faster (four fold) alkalinization reaction rate (see Fig. S3, ESI†), giving rise to self-accelerated gelations.

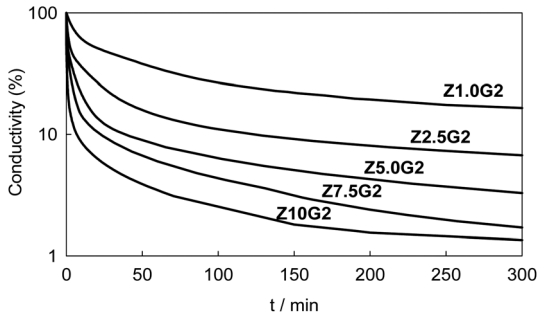

Fig. 2 Conductivity (expressed as percentage of the initial value) as a function of time.

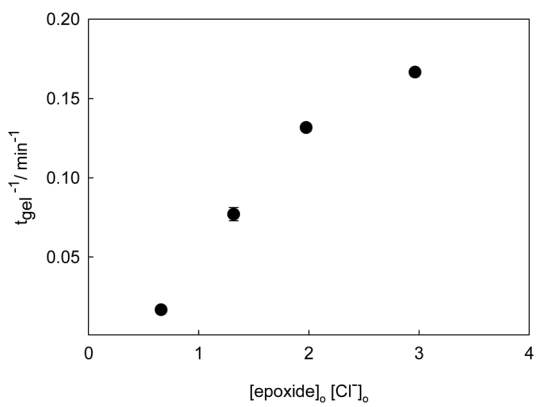

Fig. 3 Inverse of gelation time of samples as a function of the product of initial chloride and epoxide concentration, $[epoxide]_o[Cl^-]_o$.

For the particular case of sample Z2.5G2, gelation times were non-reproducible and in most of the cases the hydrogels totally reverted to the sol condition, indicating a significant hydrolysis of the chlorohydrin and the subsequent acidification (see Fig. S1, ESI†).

Interestingly, despite the wide range of initial compositions (and gelation times), all the samples resulted in highly transparent hydrogels or sols, irrespective of the reagent or solvent ratio. Hydrogels prepared with $ZrOCl_2$ concentrations of 0.40 M or higher remain stable and transparent for years with neither cracks nor noticeable syneresis. Native hydrogels (see Fig. S4, ESI†) exhibited a very small scattering, reaching the optical quality obtained by alkoxide-based routes.[8] After proper drying, transparent and robust xerogels can be obtained (see Fig. S5, ESI†).

Similar behaviour was observed in additional samples prepared with water volume fractions ranging from 30 to 85%. PXRD analysis of washed and dried samples revealed that the solid consists of ill crystallized ZrO_2, with main reflections positioned in the angular range expected for cubic or tetragonal zirconia, in excellent agreement with previous reports (see Fig. S6, ESI†).[25] Further annealing at 1273 K developed the transition to the monoclinic phase, with only traces of the starting ones.

3.3. Structural evolution of hydrogels

The representative samples were inspected by SAXS as a function of time. Fig. 4 presents the SAXS profile evolution for samples with the identical epoxide/Zr(IV) ratio and increasing Zr(IV) contents. Samples Z1.0G2, Z5.0G2 and Z7.5G2 share a common behavior in which a main signal continuously grows and displaces from initial q values around 2 nm^{-1} to a final signal centered at a fourth of this value. For sample Z10G2, fast gelation (before the initial pattern recording) prevents the observation of high q maxima values.

The microstructure of hydrogels, mainly based on silica, has been extensively studied by scattering techniques (neutrons, X-ray, light). In a previous work, we modeled the microstructure of silica hydrogels as formed by the aggregation of small particles into clusters, determining a structure that can be assimilated to a mass fractal of dimension D.[31] Dealing with the samples prepared by a sol gel route in the Zr *n*-propoxide–acetylacetone–water–*n*-propanol system, Silva *et al.*[32] found that the fractal model was appropriate to describe the texture of both hydrogels and aerogels derived from them. It is worth noting that in these cases, the log–log SAXS profiles exhibit an asymptotic behavior at high q-values, close to $I(q) \approx q^{-D}$, from which the fractal dimension, D, is derived. In the present study, we did not find a constant slope supporting the application of such a model. Instead, SAXS profiles exhibit a marked peak that shifts progressively to lower q-values as the reaction proceeds and/or the hydrogels are aged. This is indicative of the increase in size of a characteristic construction unit composing the structure and the characteristic domain size (parameter d) was analyzed by means of the Teubner and Strey phenomenological model.[33] This model was

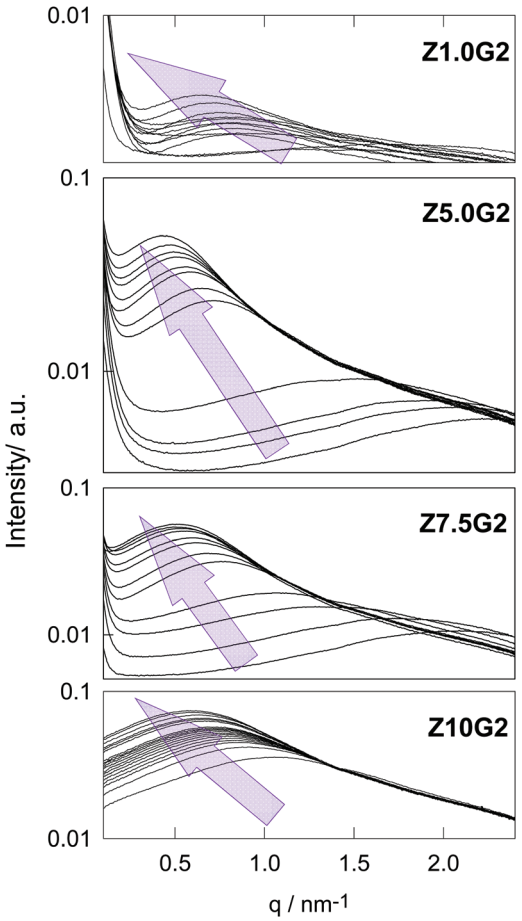

Fig. 4 Evolution of SAXS profiles with time for samples prepared with increasing Zr(IV) contents, as specified in each graph. Time evolves in the direction of the arrow; the total time intervals explored for each sample are depicted in Fig. 5 (left panel).

originally developed to describe the scattering from bi-continuous micro-emulsions, and has been successfully applied to epoxide-based hydrogels.[34]

For all the gelled samples, the process can be interpreted in terms of a sol–gel transition. A homogeneously nucleated sol composed of 2 nm primary particles continuously grows up to a critical size of 5–6 nm, when gelation takes place. Finally, these particles reach a size of 8–10 nm, depending on the Zr(IV) concentration (see Fig. 5). The more concentrated the solution, the faster the growth and the smaller the final size. If the growth process is presented as a function of conductivity, the gelled samples share a common trend. Once the conductivity decays to 40% of the starting value, nucleation takes place; around 20% the sol–gel transition is reached.

Before this event, the decay of conductivity can be interpreted in terms of polymerization. It is known that $ZrOCl_2$ salt, constituted of tetrameric units, evolves in acid media from low charge $[Zr_4(OH)_8(H_2O)_{16}Cl_6]^{2+}$ clusters to neutral polynuclear (dimers) as $[Zr_8(OH)_{20}(H_2O)_{24}Cl_{12}]$; these moieties, under alkalinization, give rise to larger polymers.[35]

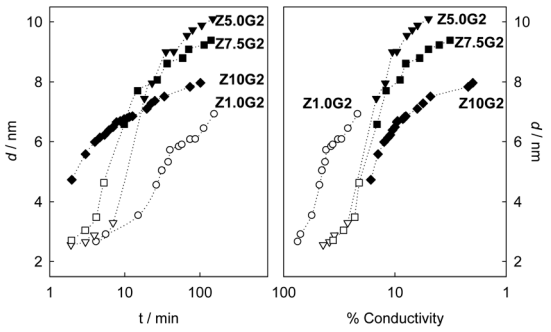

Fig. 5 Evolution of the particle diameter, *d*, as a function of time (left panel) and conductivity, expressed as the percentage with respect to the initial value (right panel). For each sample, open and filled symbols indicate the sol and the gel conditions, respectively.

It was reported that well-developed 5 nm-long ZrO_2 single crystals resulting from solvothermal procedures result in much sharper patterns than those observed herein.[36] The lack of well-defined reflections in PXRD suggests that the present nanoparticles consist of aggregated polymers with only incipient crystalline order, in agreement with the scanning microscopy images (see Fig. S7, ESI†).

4. Conclusions

Robust and highly transparent ZrO_2-water-glycerol hydrogels were obtained in a mild one-pot procedure, employing a wide range of total Zr(IV) concentrations or water to glycerol ratios. Conductivity measurements offer a fast assessment of the reaction rate; however, concentrated samples result in self-accelerated kinetics due to heat release. The mild conditions employed herein prevent massive ripening and recrystallization leaving *quasi* amorphous ZrO_2 nanoparticles with extremely low undesired visible light scattering. SAXS inspection revealed a bi-continuous like structure, suggesting that the primary particles are well interconnected in a network with no larger clusters or aggregates, ensuring a robust and translucent structure.

Acknowledgements

This work was supported by Universidad de Buenos Aires (UBACyT 20020130100610BA), Agencia Nacional de Promoción Científica y Tecnológica (ANPCyT PICT 2013 2045 and 2012 1167) and Consejo Nacional de Investigaciones Científicas y Técnicas (CONICET PIP 11220110101020). VO acknowledges CONICET for a doctoral fellowship and ALN for permanent encouragement. MP and MJ are Research Scientists of CONICET (Argentina). This work has been supported by the Brazilian Synchrotron Light Laboratory (LNLS, Brazil, proposal D11A-SAXS-6039 and D11A-SAXS1-18927). We deeply acknowledge the fruitful corrections of reviewers.

Notes and references

1 C. J. Brinker and G. W. Scherer, *Sol–Gel Science: The Physics and Chemistry of Sol–Gel*, Academic Press, 1990.
2 N. Nassif and J. Livage, *Chem. Soc. Rev.*, 2011, **40**, 849–859.
3 D. Avnir, S. Braun, O. Lev and M. Ottolenghi, *Chem. Mater.*, 1994, **6**, 1605–1614.
4 G. Carturan, R. Dal Monte, G. Pressi, S. Secondin and P. Verza, *J. Sol–Gel Sci. Technol.*, 1999, **13**, 273–276.
5 N. Nassif, O. Bouvet, M. N. Rager, C. Roux, T. Coradin and J. Livage, *Nat. Mater.*, 2002, **1**, 42–44.
6 M. L. Ferrer, L. Yuste, F. Rojo and F. Del Monte, *Chem. Mater.*, 2003, **15**, 3614–3618.
7 M. Perullini, M. Jobbagy, G. Soler-Illia and S. A. Bilmes, *Chem. Mater.*, 2005, **17**, 3806–3808.
8 M. Perullini, M. Jobbagy, M. Berudez Moretti, S. Correa Garcia and S. A. Bilmes, *Chem. Mater.*, 2008, **20**, 3015–3021.
9 Y. Ferro, M. Perullini, M. Jobbagy, S. A. Bilmes and C. Durrieu, *Sensors*, 2012, **12**, 16879–16891.
10 M. Perullini, Y. Ferro, C. Durrieu, M. Jobbagy and S. A. Bilmes, *J. Biotechnol.*, 2014, **179**(1), 65–70.
11 M. Perullini, M. Jobbagy, N. Mouso, F. Forchiassin and S. A. Bilmes, *J. Mater. Chem.*, 2010, **20**, 6479–6483.
12 A. Lèonard, P. Dandoy, E. Danloy, G. Leroux, C. F. Meunier, J. C. Rooke and B. L. Su, *Chem. Soc. Rev.*, 2011, **40**, 860–885.
13 M. Perullini, M. M. Rivero, M. Jobbágy, A. Mentaberry and S. A. Bilmes, *J. Biotechnol.*, 2007, **127**, 542–548.
14 M. Amoura, N. Nassif, C. Roux, J. Livage and T. Coradin, *Chem. Commun.*, 2007, **39**, 4015–4017.
15 M. Amoura, R. Brayner, M. Perullini, C. Sicard, C. Roux, J. Livage and T. Coradin, *J. Mater. Chem.*, 2009, **19**, 1241–1244.
16 M. Perullini, M. Amoura, M. Jobbagy, C. Roux, J. Livage, T. Coradin and S. A. Bilmes, *J. Mater. Chem.*, 2011, **21**, 8026–8031.
17 A. E. Gash, T. M. Tillotson, J. H. Satcher, L. W. Hrubesh and R. L. Simpson, *J. Non-Cryst. Solids*, 2001, **285**, 22–28.
18 A. E. Gash, T. M. Tillotson, J. H. Satcher, J. F. Poco, L. W. Hrubesh and R. L. Simpson, *Chem. Mater.*, 2001, **13**, 999–1007.
19 Y. Tokudome, N. Tarutani, K. Nakanishi and M. Takahashi, *J. Mater. Chem. A*, 2013, **1**, 7702–7708.
20 N. Tarutani, Y. Tokudome, M. Fukui, K. Nakanishi and M. Takahashi, *RSC Adv.*, 2015, **5**, 57187–57192.
21 N. Tarutani, Y. Tokudome, K. Nakanishi and M. Takahashi, *RSC Adv.*, 2014, **4**, 16075–16080.
22 C. N. Chervin, B. J. Clapsaddle, H. W. Chiu, A. E. Gash, J. H. Satcher and S. M. Kauzlarich, *Chem. Mater.*, 2005, **17**, 3345–3351.
23 C. N. Chervin, B. J. Clapsaddle, H. W. Chiu, A. E. Gash, J. H. Satcher and S. M. Kauzlarich, *Chem. Mater.*, 2006, **18**, 4865–4874.
24 O. C. Bujor, S. Celerier and S. Brunet, *J. Sol–Gel Sci. Technol.*, 2010, **54**, 220–231.
25 L. Zhong, X. Chen, H. Song, K. Guo and Z. Hu, *RSC Adv.*, 2014, **4**, 31666–31671.
26 K. V. Schubert, R. Strey, S. R. Kline and E. W. Kaler, *J. Chem. Phys.*, 1994, **101**, 5343–5355.
27 J. N. Brönsted, M. Kilpatrick and M. Kilpatrick, *J. Am. Chem. Soc.*, 1929, **51**, 428–461.
28 W. L. Petty and P. L. Nichols, *J. Am. Chem. Soc.*, 1954, **76**, 4385–4389.
29 V. Oestreicher, I. Fábregas and M. Jobbágy, *J. Phys. Chem. C*, 2014, **118**, 30274–30281.
30 V. Oestreicher and M. Jobbágy, *Langmuir*, 2013, **29**, 12104–12109.
31 M. Perullini, M. Jobbagy, S. A. Bilmes, I. L. Torriani and R. Candal, *J. Sol–Gel Sci. Technol.*, 2011, **59**, 174–180.
32 M. C. Silva, G. Trolliard, O. Masson, R. Guinebretiere, A. Dauger, A. Lecomte and B. Frit, *J. Sol–Gel Sci. Technol.*, 1997, **8**, 419–424.
33 M. Teubner and R. Strey, *J. Chem. Phys.*, 1987, **87**, 3195–3200.
34 I. Krakovsky and N. K. Szekely, *Eur. Polym. J.*, 2015, **71**, 336–351.
35 A. Singhal, L. M. Toth, J. S. Lin and K. Affholter, *J. Am. Chem. Soc.*, 1996, **118**, 11529–11534.
36 R. Si, Y. W. Zhang, S. J. Li, B. X. Lin and C. H. Yan, *J. Phys. Chem. B*, 2004, **108**, 12481–12488.